High-order-harmonic generation from Rydberg atoms driven by plasmon-enhanced laser fields

Y. Tikman,[1,*] I. Yavuz,[1] M. F. Ciappina,[2] A. Chacón,[3] Z. Altun,[1] and M. Lewenstein[3,4]

[1]*Physics Department, Marmara University, Ziverbey, 34722 Istanbul, Turkey*

[2]*Max-Planck-Institut für Quantenoptik, Hans-Kopfermann-Strasse 1, 85748 Garching, Germany*

[3]*Institut de Ciències Fotòniques (ICFO), The Barcelona Institute of Science and Technology, Avenida Carl Friedrich Gauss 3, 08860 Castelldefels (Barcelona), Spain*

[4]*Institució Catalana de Recerca i Estudis Avançats (ICREA), Lluis Companys 23, 08010 Barcelona, Spain*

(Received 1 June 2015; published 10 February 2016)

We theoretically investigate high-order-harmonic generation (HHG) in Rydberg atoms driven by spatially inhomogeneous laser fields, induced, for instance, by plasmonic enhancement. It is well known that the laser intensity should exceed a certain threshold in order to stimulate HHG when noble gas atoms in their ground state are used as an active medium. One way to enhance the coherent light coming from a conventional laser oscillator is to take advantage of the amplification obtained by the so-called surface plasmon polaritons, created when a low-intensity laser field is focused onto a metallic nanostructure. The main limitation of this scheme is the low damage threshold of the materials employed in the nanostructure engineering. In this work we propose the use of Rydberg atoms, driven by spatially inhomogeneous, plasmon-enhanced laser fields, for HHG. We exhaustively discuss the behavior and efficiency of these systems in the generation of coherent harmonic emission. Toward this aim we numerically solve the time-dependent Schrödinger equation for an atom, with an electron initially in a highly excited nth Rydberg state, located in the vicinity of a metallic nanostructure. In this zone the electric field changes spatially on scales relevant for the dynamics of the laser-ionized electron. We first use a one-dimensional model to investigate systematically the phenomena. We then employ a more realistic situation, in which the interaction of a plasmon-enhanced laser field with a three-dimensional hydrogen atom is modeled. We discuss the scaling of the relevant input parameters with the principal quantum number n of the Rydberg state in question and demonstrate that harmonic emission can be achieved from Rydberg atoms well below the damage threshold, thus without deterioration of the geometry and properties of the metallic nanostructure.

DOI: 10.1103/PhysRevA.93.023410

I. INTRODUCTION

High-order-harmonic generation (HHG) has been extensively studied, both theoretically and experimentally, considering its potential for synthesizing bright isolated XUV pulses, which are the workhorse to understand ultrafast electron dynamics, on the subfemtosecond and subangstrom spatiotemporal scale [1,2]. The dynamics of HHG is transparently described by the so-called three-step model [3,4]. We summarize the sequence as follows: (i) a bound electron tunnels out from the Coulomb barrier, suppressed by the incident laser electric field; (ii) this laser-ionized electron accelerates in the continuum under the sole influence of the electric field; and (iii) the electron is driven back towards the parent ion and converts its kinetic energy in energetic and coherent photons upon recombination. The maximum photon energy achievable from the HHG process is determined by the classical cutoff law $\omega_{\text{cutoff}} = I_p + 3.17U_p$ [3,4], where the ponderomotive potential U_p is $\sim I\lambda^2$ (I and λ being the peak intensity and wavelength of the incident laser field, respectively) and I_p is the ionization potential of the target atom of interest.

The relationship $\omega_{\text{cutoff}} \propto I\lambda^2$ suggests two main routes to obtaining high-energetic coherent photons, namely, (i) to increase the laser intensity I and (ii) to use laser sources with longer wavelengths. Several limitations in both schemes are in order. On one hand, ionization clearly rises for higher laser intensities, which, already at the level of the single-atom response, dramatically decreases the probability of electron recombination responsible for emission of photons of a high frequency: in effect there is no HHG above the, so-called, saturation intensity I_{sat} (cf. [5]). Moreover, other instrumental control parameters needed to obtain an appreciable photon flux, such as phase matching between the atomic emitters (for details see, e.g., [6] and [7]), are affected by higher ionization levels. The other pathway, the utilization of longer wavelengths, suffers from disadvantages as well. For instance, it is demonstrated that the HHG yield scales as $\lambda^{-(5\sim6)}$, and as a consequence, it appears to be challenging to obtain a measurable signal as λ increases due to this poor conversion efficiency [8].

In an ordinary HHG experiment, a supersonic jet of noble-gas atoms, all in their ground states ($I_p \sim 15$–30 eV), is used as a target. When near-infrared lasers ($\lambda \sim 700$–2000 nm) lasers are employed, the minimum laser intensity to observe the HHG phenomenon lies in the range of $\sim 10^{12} - 10^{13}$ W/cm^2, which often requires a second-stage amplification at the output of a conventional femtosecond laser oscillator (with typical output intensities in the range of $\sim 10^{10} - 10^{11}$ W/cm^2). Considering the large infrastructure needed for this amplification phase, many alternative schemes have been proposed to amplify the incident field so as to permit an efficient strong field-matter interaction [9,10]. One that has received great interest recently is the so-called plasmon-enhanced HHG [11–16]. This approach takes advantage of the field enhancement generated when a laser field of moderated intensity is focused on an array of metallic nanostructures [17].

*yavuztikman@marun.edu.tr

With this arrangement it is then possible to boost the input laser power by several orders of magnitude [12]. Here, special attention should be paid to the geometry of the nanostructure, typically a metallic bow tie of nanometric dimensions with a gap between the apexes (for details see, e.g., [12]). By fine-tuning the spatial metal geometry or the gap distance of the nanostructure elements, which act like point sources, it is possible to amplify an incident field with a *moderate* intensity ($\sim 10^{11}$ W/cm^2) up to the intensities needed to produce XUV emission from atomic gas targets [12,16].

Due to the confinement of the incoming field in a nanovolume, the resulting plasmon-enhanced field typically presents spatial variation on a nanometer scale. For instance, within a gap of roughly 20 nm, the intensity of the input field is enhanced a few orders of magnitude at the gap center, drastically increases, and culminates in a maximum near the metal surface [12]. Due to this field gradient and the electron confinement in a small volume, the conventional Keldysh picture of strong-field physics—in which the spatial dependence of the laser field and the Coulomb potential influence is ignored—is incapable of fully explaining the underlying physics [18–20]. As a result, there has been an intense effort both to comprehend the fundamental physics at the microscopic level and to numerically simulate the processes at a multiscale level [16,20–30]. Elucidating the mechanisms behind plasmon-enhanced HHG is thus essential due its potential technological applications (e.g., see [31]).

Since the first realization of HHG from plasmon-enhanced fields by bow-tie-shaped nano-antennas, a few alternative nanosystems have been explored in order to optimize as well as to modify the phenomenon through the synergy between experiments and theory. Among these systems we could cite coupled ellipsoids [32], tapered nanocones [13,33], metal nano-particles [34], and nanocomposites [35,36]. However, despite its initial meteoric success and promise, the plasmon-enhanced harmonic emission process still suffers in many aspects, such as the melting of the metallic nanostructures caused by the high buildup intensities near the metal surface and the impossibility of disentangling the emission of coherent and incoherent light [14,37]. Additionally, the low conversion efficiency, due to the low target-gas density contributing to the photoemission, makes it challenging to increase the signal-to-noise ratio and to unravel the emission from the noble-gas atoms from that coming directly from the metallic nanoantenna [15,33]. On the other hand, there are apparent discrepancies between the intensity enhancements predicted through finite-element simulations and those that are necessary for efficient HHG as estimated by the conventional three-step model [38]. Because of these circumstances, the feasibility of using metallic nanostructures to drive HHG is actively debated in the literature [14,37,39]. Having these complications in mind, our main purpose is to address an alternative way to obtain efficient HHG while avoiding the damage to the nanostructure elements caused by the high-intensity plasmon-enhanced fields.

One way to decrease the intensity needed for efficient HHG is to prepare atoms in their excited states, which are characterized by smaller values of I_p. The price one has to pay, however, is that the HHG cutoff will decrease, in accordance with the classical law $\omega_{\text{cutoff}} = I_p + 3.17U_p$, where both U_p and the associated saturation intensity I_{sat} must necessarily be lower. Alternatively, this obstacle can be circumvented and an enhanced cutoff obtained by considering HHG originating from the superposition of an excited and a ground state in atoms [40,41] or excited vibrational states in molecules [42]; for more recent developments of these ideas see [43–45]. Another, and much easier pathway, is to scale the laser intensity and wavelength (frequency) in accordance with I_p. We adopt the latter strategy in this paper.

Owing to their loosely bound valence electrons, Rydberg atoms are highly sensitive to external influences which can easily cause them to ionize [46]. In other words, while high-intensity fields are required to ionize an atom in its ground state, where the principal quantum number $n = 1$, the intensity required to ionize a Rydberg atom, $n \gg 1$, is considerably lower. Here, the scaling of Rydberg atoms with n offers insights into their peculiar features [46]. As shown in many studies, the relevant parameters here, e.g., the ionization potential I_p, the radius of the nth Rydberg orbit r_R, the electric-field strength E_R felt by an electron at the nth Rydberg orbit, and the energy level spacing ΔE_R, the latter leading to even more closely spaced levels as n increases (see below), scale with n as

$$I_p = n^{-2}\widetilde{I_p}, \tag{1}$$

$$r_R = n^2\widetilde{r}, \tag{2}$$

$$E_R = n^{-4}\widetilde{E_0}, \tag{3}$$

and

$$\Delta E_R = n^{-3}\widetilde{\Delta E_0}, \tag{4}$$

where the quantities with tildes correspond to the values for $n = 1$.

Thus, if one applies an intense laser field to Rydberg atoms and attempts to study the atomic response as a function of n, it is natural to consider the n scaling of the relevant electron dynamics parameters based on the above equations. According to this approach, if the ionization potential scales as in Eq. (1), the laser electric field as we consider higher n values should scale as

$$E_0 = n^{-4}\widetilde{E_0} \tag{5}$$

and the laser frequency as

$$\omega_0 = n^{-3}\widetilde{\omega_0}, \tag{6}$$

where the quantities with tildes correspond now to characteristic values of the laser field and frequency used for $n = 1$. In such a situation, for instance, the ponderomotive potential $U_p = E_0^2/4\omega_0^2$ scales as n^{-2}, and thus the cutoff frequency (or maximum photon energy) ω_{cutoff} and cutoff harmonic order $q_{\text{cut}} = \omega_{\text{cutoff}}/\omega_0$ scale as n^{-2} and n, respectively. Interestingly, the Keldysh parameter $\gamma = \sqrt{I_p/2U_p}$, which separates the tunneling (for $\gamma \ll 1$) and multiphoton (for $\gamma \gg 1$) dynamical regimes, remains unscaled with n [47]. Finally, the classical quiver radius of the laser ionized electron $\alpha_0 = E_0/\omega_0^2$ scales as n^2, i.e., like the Rydberg radius r_R [see Eq. (2)].

In this paper, we address and demonstrate the behavior and the usefulness of Rydberg atoms in the plasmon-enhanced HHG process. Considering the fact that the tunnel ionization

is instrumental in the HHG process [3,6], the Rydberg atoms could be advantageous for HHG driven by plasmon-enhanced fields generated by metallic nanostructures, since relatively low intensities are required to detach Rydberg electrons via the tunneling processes. This fact could—potentially—prevent the damage and melting of the employed nanostructures during the HHG process.

In the experiments performed in plasmon-enhanced HHG, the target atoms—mostly in their ground states—are directly injected onto the nanostructure through a gas jet [12,16]. If we want to drive atoms in an excited n state, on the other hand, an extra preinjection or preparatory scheme or mechanism is needed, which could potentially be a dye laser with a high repetition (MHz) rate, but one should stress that in a general context several schemes of this sort were discussed in the literature recently (for schemes based on adiabatic passage see [48–51] and for pump-probe schemes see, e.g., [45]). After the injection, the survival of the atoms in their excited states is an issue that should be considered. However, typically the lifetime of Rydberg atoms due to spontaneous decay or background microwave ionization is in the microsecond (10^{-6} s) range [46], i.e., much longer than the strong-field ultrashort processes considered here, typically developed on the subfemtosecond (10^{-15} s) time scale. Moreover, Bleda *et al.* [47] have shown that the field-effect ionization rate dramatically decreases with increasing n. Thus, the strongest contribution to the ionization and HHG process comes directly from the initially prepared excited n-state atoms. Accordingly, we could anticipate that the Rydberg atoms, injected into the nanogap region, can largely survive during the strong-field interaction process.

We employ the numerical solution of the time-dependent Schrödinger equation (TDSE), in both one dimension and three dimensions, to compute the HHG spectra of an atom in a plasmon-enhanced linearly polarized laser field. To avoid any misunderstanding we stress that this paper is not about the determination of the plasmon-enhanced fields, which is another important and challenging problem. Here we assume a certain spatial form and strength for the plasmon-enhanced fields and they are treated as a given external field. Still these fields can and are controlled in experiments by changing the laser intensity, wavelength, or polarization or by fine-tuning the properties and geometry of the metallic nanostructure.

In this contribution we systematically study the atomic response when we alter the initial target-atom bound state. We increase the principal quantum number of the initial Rydberg state n and n-scale the relevant field parameters accordingly. In our simulations, we assume a bow-tie-shaped nanoantenna as our plasmon-enhanced field source, since this particular case has been extensively investigated [11–16]. However, our approach could, in principle, be extended to any nanostructure element whose spatiotemporal profile is analogous to the bow-tie nanoantenna one. At the same time we stress that in the explicit calculations we use a "caricature" of the true spatial dependence of the plasmon-enhanced field, assuming that locally, in the vicinity of the considered atom, it depends linearly on the space coordinates. It should be noted, however, that this simple approximation grabs the main effects of the electric-field inhomogeneity in space; for a more careful description of plasmon-enhanced fields see, for instance, Refs. [52] and [53], where finite-difference time-dependent codes were used to solve the Maxwell equations to determine the accurate shape and form of the spatially inhomogeneous fields.

We also emphasize that here the calculations are restricted to $n \leq 8$ since the span of the electron wave packet (quiver radius) is of the order of the gap size ($\sim$ 20 nm) for typical laser parameters. For $n > 8$, on the other hand, the continuum electron could reach the metal surfaces and be absorbed. Finally, we assume that the field-enhancement factor is kept constant as the field intensity and laser frequency are n-scaled.

The paper is organized as follows. In Sec. II, we describe our theoretical methodologies for simulating the HHG process from Rydberg atoms driven by plasmon-enhanced fields. First, in Sec. II A, the one-dimensional (1D) model, based on the 1D TDSE, is presented. Next, in Sec. II B, a more realistic approach, based on the solution of a three-dimensional (3D) TDSE, is introduced. In Sec. III we present results using our 1D model atom. On the one hand, in Sec. III A, we simulate the electron wave-packet dynamics and obtain plasmonic HHG from Rydberg atoms with *fixed* laser-field parameters (i.e., unscaled field amplitude E_0 and frequency ω_0). On the other hand, in Sec. III B, the simulations are performed for n-scaled E_0 and ω_0. Finally, in Sec. III C, we compare the HHG yields obtained in both Sec. III A and Sec. III B and discuss their main features, similarities, and differences. Section IV is focused on the TDSE simulations in three dimensions. Here, we model an H atom interacting with a plasmon-enhanced laser field and compute the HHG spectra for different laser parameters and excited states. In order to complete the analysis, in Sec. V we perform semiclassical simulations, based on the three-step model. We conclude our contribution in Sec. VI.

II. METHODOLOGY

We investigate the mechanism of plasmonic HHG from Rydberg atoms through the numerical solution of the TDSE. The interaction of a target atom with a plasmon-enhanced linearly polarized laser field is modeled via two approaches; a 1D model atom and a real hydrogen atom in three dimensions. Below we provide the details of these two methodologies.

A. Model hydrogen in one dimension

Since the dynamics of the atomic electron in a strong laser field is mainly along the direction of the field (in a linearly polarized laser pulse), it is reasonable to model the HHG in a 1D spatial dimension [54]. The TDSE describing the interaction of a 1D model atom with a laser field is written as follows (atomic units are used throughout the article unless otherwise stated):

$$i\frac{\partial}{\partial t}\psi(x,t) = \left[-\frac{1}{2}\frac{\partial^2}{\partial x^2} + V(x) + xE(x,t)\right]\psi(x,t). \quad (7)$$

Here the model soft-core potential is taken as $V(x) = -1/\sqrt{2+x^2}$. From the field-free solutions $\psi_n(x)$ of the Schrödinger equation for the 1D model atom, one can find that the ionization potential of the ground state is $I_p = 0.5$ a.u.

and the energy levels follow

$$E_n = \frac{-a}{(n+b)^2}, \tag{8}$$

where the parameters a and b can be found by fitting the time-independent solutions of Eq. (7). Although only the ground-state energy matches that of a real hydrogen atom, the Rydberg-like character of the bound-state energies for high n values (i.e., $E_n \sim n^{-2}$ for $n \gg 1$) implies that the scaling rules discussed in Sec. I are still valid for this 1D model atom [55]. Taking the center of the nanovolume as the coordinate origin, the spatiotemporal profile of the laser field, represented by $E(x,t)$, is assumed to be in the form [21–23]

$$E(x,t) \simeq E(t)[1 + h(x)], \tag{9}$$

where the space-free portion of the electric field is $E(t) = E_0 f(t)\cos(\omega_0 t)$. E_0 and ω_0 are the peak amplitude [$E_0 = \sqrt{I/I_0}$ (a.u.) with $I_0 = 35.1$ PW/cm^2] and the frequency of the driving laser electric field, respectively. $f(t)$ defines the pulse envelope and is taken as a flat-top shape 20 cycles long with 1-cycle ramp-up and -down. In Eq. (9) $h(x)$ represents the functional form of the plasmon-enhanced field. One of the main advantages of the 1D model is that it allows us to include any functional form for $h(x)$ (for different examples see, e.g., [22], [34], and [52]). Nevertheless, it is often sufficient to approximate $h(x)$ by a linear dependence, i.e., $h(x) \simeq \beta x$, where β defines the region of spatial inhomogeneity of the field. Therefore, β has the units of inverse length. Results have shown that β is an instrumental parameter for controlling the laser-induced dynamics of the ionized electrons and, consequently, the modifications observed in the spectral profile of plasmonic HHG [21–23].

B. Real hydrogen in three dimensions

We also employ the numerical solution of the TDSE of a hydrogen atom in three dimensions interacting with a linearly polarized, in the z axis, plasmon-enhanced laser field. The TDSE in the length gauge can be written as

$$i\frac{\partial\psi(\mathbf{r},t)}{\partial t} = \left[-\frac{\nabla^2}{2} + V(r) + zE(z,t)\right]\psi(\mathbf{r},t), \tag{10}$$

where $V(r) = -1/r$ is the atomic potential for the H atom. Here, the spatiotemporal profile of the laser field is taken to be similar to the one we used for the 1D model atom, i.e., $E(z,t) = E_0 f(t)(1+\beta z)\cos(\omega_0 t)$. However, this time we use a $\sin^2$-shaped pulse with a total duration of four cycles. The details of the 3D TDSE numerical solution for a H atom in a plasmon-enhanced laser field can be found in Refs. [20] and [23]. In addition, the 3D TDSE is able to model with precision any atom within the single-active-electron (SAE) approximation (see, e.g., [24] for the He atom) by adequately tuning the atomic potential $V(r)$. Mention of two disadvantages of the 3D TDSE model is in order, namely, (i) the high computational cost and (ii) the complications of modeling a general spatial shape for the plasmon-enhanced field (to the best of our knowledge, only the linear case has been modeled). Since the energy levels of the H atom scales as n^{-2}, the scaling laws provided in Sec. I exactly apply.

For both the 1D and the 3D simulations, boundary reflection mask functions of the form $\cos^{1/8}$ multiply the electron wave function at each time step in order to avoid spurious reflections [56]. The harmonic yield is then calculated from the modulus square of the Fourier transform $a(\omega)$ of the dipole acceleration $a(t)$ [57], i.e.,

$$D(\omega) = |a(\omega)|^2 \tag{11}$$

$$= \left|\frac{1}{T_p}\frac{1}{\omega^2}\int_{-\infty}^{\infty} dt e^{-i\omega t} a(t)\right|^2, \tag{12}$$

where T_p is the total duration of the laser pulse (for more details see, e.g., [22]).

Furthermore, the spatial dependence of the field enhancement in Eq. (9) is known to be an approximate expression, versus the realistic field enhancement [21,34,52]. However, in many theoretical studies, Eq. (9) has been shown to be sufficient to elucidate the underlying physics of the problem of interest [16,20–30].

III. PLASMONIC HHG FROM RYDBERG STATES OF A 1D MODEL ATOM

A. Plasmonic HHG with unscaled field parameters

In this section, we examine plasmonic HHG from the Rydberg series of a 1D model atom. We employ $n = 1 - 8$ for an *unscaled* laser intensity I and frequency ω_0. Here we take $I = 20$ TW/cm^2 (1 TW/cm$^2 = 1 \times 10^{12}$ W/cm^2) and $\lambda = 800$ nm, i.e., $\omega_0 = 0.057$ a.u. (photon energy, 1.55 eV). The field inhomogeneity parameter β is taken as 0.016 a.u., corresponding to a factor of ~ 15 intensity enhancement near the metallic surface, i.e., 10 nm away from the gap center, which is similar to that reported by Kim *et al.* [12] (note that this is an additional enhancement on top of the increase generated by the surface plasmon polaritons).

For demonstration purposes, Figs. 1(a)–1(c) show results only for $n = 1$, 4, and 8, respectively. First, for $\beta = 0$, i.e., for the spatially homogeneous case, the cutoff position for the $n = 1$ state is found to be $q_{\text{cut}} = 11$ (which corresponds to an $\omega_{\text{cutoff}} = 17.4$ eV) using the three-step model [3,4]. As shown in Fig. 1(a), the HHG cutoff is extended by a factor of roughly 2 to $q_{\text{cut}} = 23$ (corresponding to an $\omega_{\text{cutoff}} = 35.6$ eV), when the field inhomogeneity parameter is $\beta = 0.016$ a.u. The increase in the HHG cutoff with $\beta \neq 0$ is consistent with previous theoretical studies [16,20–30].

The increase in the HHG cutoff originates from the further acceleration of the ionized electron moving in the plasmon-enhanced laser field. This results in a ponderomotive potential boost, due to the increase in the field strength as a function of the increasing spatial coordinate x [21,23]. Since the highest harmonic photon energy depends on I_p and U_p [3], the larger is U_p, the higher the ω_{cutoff} that will be reached. One can also see the appearance of both odd and even harmonics up to the HHG cutoff and below, which is attributed to the breaking of inversion symmetry owing to the spatial inhomogeneity of the plasmon-enhanced field [21,22]. Beyond $n = 1$ we find that the profiles of the harmonic spectra are very similar for $n = 2$–8,

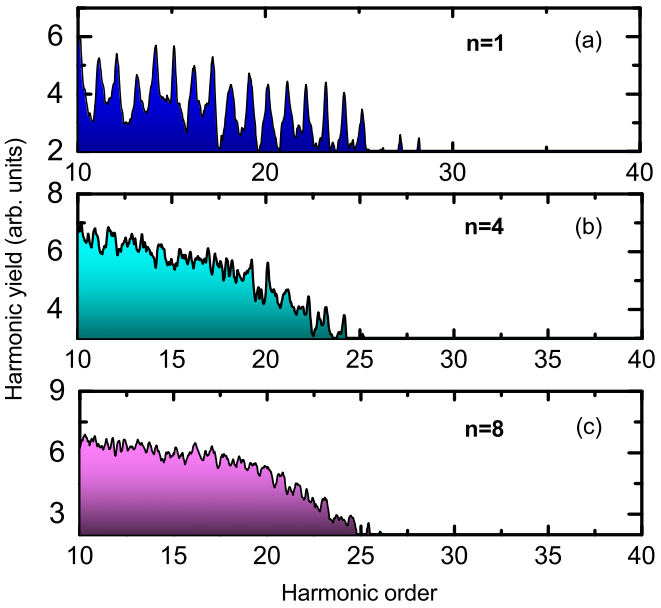

FIG. 1. Plasmonic-HHG harmonic yield vs harmonic order (ω/ω_0) from n states obtained with a 1D model atom. Here, the $n = 1$, 4, and 8 states are presented. $I = 20$ TW/cm^2 (1 TW/cm^2 = 1×10^{12} W/cm^2) and $\lambda = 800$ nm are used in all cases. The parameter β is chosen as 0.016 a.u.

namely, they appear to be independent of the n state [the $n = 4$ and 8 cases are shown in Figs. 1(b) and 1(c), respectively].

In Fig. 2 we depict the maximum photon energy (ω_{cutoff}) by varying the n state for both spatially homogeneous ($\beta = 0$) and spatially inhomogeneous ($\beta = 0.016$ a.u.) fields; the ω_{cutoff} drops significantly with n for $\beta = 0$ and converges at an $\omega_{\text{cutoff}} = 3.8$ eV, which corresponds to $3.17U_p$ ($U_p = 1.19$ eV). In contrast, beyond the $n = 1$ state, ω_{cutoff} oscillates with a narrow energy band around $5\omega_0$ above the conventional case for $\beta = 0.016$ a.u. The modest dependence of ω_{cutoff}, as well as the conversion efficiency of the n state ($n > 1$) for $\beta \neq 0$, could be attributed to the ionization dynamics and electron confinement during propagation, which strongly correlate with the maximum photon energy and harmonic efficiency [3].

The threshold intensity for the barrier-suppression ionization (BSI), I_{BSI}, for a classical electron of a hydrogen-like

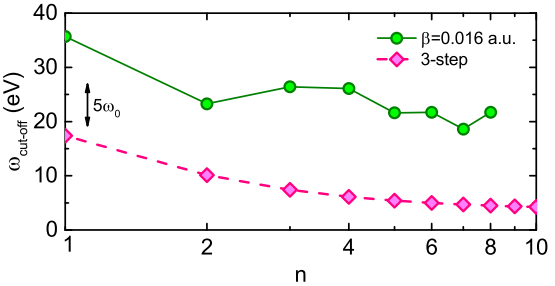

FIG. 2. Variation of the ω_{cutoff} of plasmonic HHG ($\beta = 0.016$ a.u.) with n for fixed values of E_0 and ω_0. The dashed line shows the predictions of the three-step model [3,4].

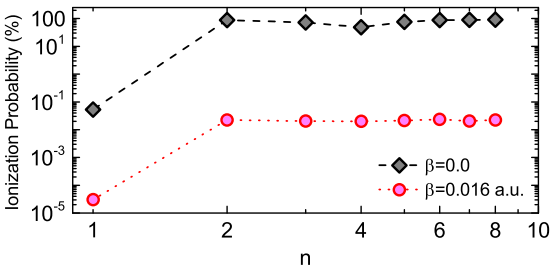

FIG. 3. Ionization probability as a function of the n state for *unscaled* field parameters, E_0 and ω_0. Note that the ionization saturates beyond $n = 2$ for both cases. Due to the possibility of electron confinement via repulsive forces (towards the nucleus) the ionization is largely suppressed in all n cases with $\beta = 0.016$ a.u.

atom in a circular orbit, is defined by

$$I_{\text{BSI}} = 6.02 \times 10^3 |E_n\,[\text{a.u.}]|^3\ \text{TW/cm}^2. \tag{13}$$

I_{BSI} defines a critical point at which the Coulomb barrier is suppressed below the bound state n with energy E_n [58,59].

The intensity value $I = 20$ TW/cm^2 we use for $n = 1$ and $\beta = 0$ is much lower than I_{BSI} ($I_{\text{BSI}} = 750$ TW/cm^2), but it is higher than that for other n states since the I_{BSI} condition in Eq. (13) scales as n^{-6}. Figure 3 clearly supports this argument. We observe that the ionization saturates beyond $n = 1$ (with almost-full ionization) for $\beta = 0$. Hence, one should not expect an efficient HHG from $n \geqslant 2$ states with homogeneous fields, because of the likelihood of no electron rescattering.

However, note that the condition given in Eq. (13) is valid only for spatially homogeneous fields, i.e., for the case of $\beta = 0$. Through numerical simulations we find that when the atom is placed in a plasmon-enhanced field, the ionization probabilities are suppressed by roughly four orders of magnitude (see Fig. 3), owing to the electron confinement via repulsive forces (towards the nucleus). Thus, the confined continuum electrons—which are likely to escape and never return close to the parent ion in the case of homogeneous fields—could be driven back, resulting in an efficient recombination with the nucleus, leading to an ultimate coherent photoemission.

Although our results appear to be promising, namely, one could attain more energetic and efficient photons through a Rydberg-series atom driven by a plasmon-enhanced laser field, the laser-field intensity increases in such a way as to exceed the damage threshold of the metallic nanostructure, and thus this procedure is not very beneficial (see Sec. I). In order to give a clearer picture, in the next section, we investigate plasmonic HHG from a Rydberg-series atom for a set of *scaled* laser-field parameters.

B. Plasmonic HHG with n-scaled field parameters

Here we study plasmonic HHG by Rydberg atoms by systematically n-scaling the input laser parameters. As n increases, the laser-field intensity I and frequency ω_0 are scaled as $20n^{-8}$ TW/cm^2 and $1.55n^{-3}$ eV, respectively. We assume that the spatial dependence of the plasmon-enhanced field is fixed, independent of the value of n. Although the field frequency critically affects the plasmonic-field enhancement,

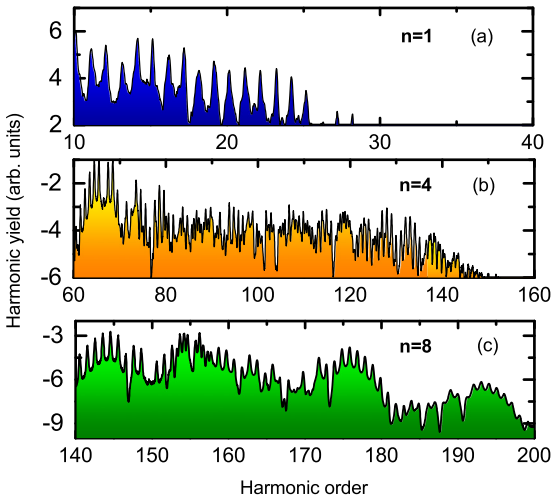

FIG. 4. Plasmonic-HHG harmonic yield vs harmonic order (ω/ω_0) for n states obtained with a 1D model atom. Field parameters are scaled as $I = 20/n^8$ TW/cm^2 and $\lambda = 800n^3$ nm for each n state. The field inhomogeneity β is chosen as 0.016 a.u.

we assume that as we n-scale ω_0, the degree of field enhancement through surface plasmon resonances is also fixed. Nonetheless, this condition could potentially be fulfilled by systematically tweaking the configuration and geometry of the nanostructure element so as to maintain the degree of field enhancement at different field laser wavelengths [60–62].

Thus, for higher values of n, the intensity enhancement in the nanostructure volume would be much lower, and as a result, reaching the nanostructure damage threshold would be highly unlikely. It has been shown that 100–1000 TW/cm^2 peak intensities are harmful to nanostructures [12–15], therefore alternatives to diminish these values would be highly desirable. These values are also valid for our set of I and β parameters, since the intensity is enhanced up to 300 TW/cm^2 near the metal's surfaces. However, we could use, for instance, $I = 0.3$ GW/cm^2 for $n = 4$. In addition, the intensity I near the metal surfaces is 4.5 GW/cm^2, which is still considerably below the damage threshold. Note that this maximum value depends on the spatiotemporal shape of the plasmon-enhanced electric-field function and the field inhomogeneity parameter β we use. In Fig. 4, we present results for $n = 1$, 4, and 8. As shown, more harmonics ω/ω_0 are covered with increasing n.

There are clear cutoffs at the 23rd, 138th, and 193rd harmonics for $n = 1$, 4, and 8, respectively. Note also that more regular and clear harmonic peaks for $n = 4$ and 8 are obtained, as opposed to the irregular ones shown in Fig. 1. Although the harmonic order of the cutoff position increases, the maximum photon energies decrease at values of 35.6, 3.3, and 0.6 eV, for $n = 1$, 4, and 8, respectively. This is so since the photon energies are given by $\omega = q\omega_0$ and ω_0 scales as n^{-3} [see Eq. (6)].

The variation of ω_{cutoff} with n (for $n = 1$–8) for both spatially homogeneous and spatially inhomogeneous laser fields is shown in Fig. 5. As can be inferred, the ω_{cutoff} for spatially homogeneous—i.e., conventional—laser fields decreases with n. This decline scales as n^{-2} since $I_p \sim n^{-2}$ for higher values of n in our 1D model atom. Our ω_{cutoff} results

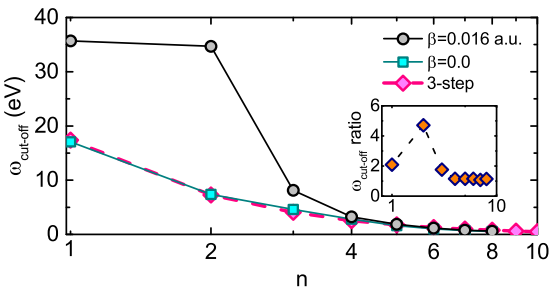

FIG. 5. Variation of the ω_{cutoff} of conventional ($\beta = 0$) and plasmonic ($\beta = 0.016$ a.u.) HHG with n for n-scaled E_0 and ω_0. The dashed line shows the predictions of the three-step model [3,4]. Inset: ω_{cutoff} enhancement, computed as the ratio $\omega_{\text{cutoff}}^{\text{plasm}}/\omega_{\text{cutoff}}^{\text{conv}}$, as a function of n.

for conventional laser fields match exactly the predictions of the three-step model, i.e., $\omega_{\text{cutoff}} = I_p + 3.17U_p$ [3,4].

We also show in Fig. 5 the variation of ω_{cutoff} with n for an atom exposed to a plasmon-enhanced field with $\beta = 0.016$ a.u. We see from Eq. (9) that the spatial intensity enhancement becomes effective once the electron wave packet is released and pushed away from the nucleus. In other words, $(1 + \beta x) \to 1$ for $x \to 0$. Therefore, to a first-order approximation, we can employ the conventional quasistatic ionization rate expressions to understand the influence of n on ionization. Quasistatic ADK ionization rates are defined by [63]

$$\Gamma \sim \exp[-2(2I_p)^{3/2}/(3E_0)], \tag{14}$$

therefore, it is clear that the $[(2I_p)^{3/2}/(3E_0)]$ term scales as n. As a result, the tunnel ionization probability drops drastically with increasing n. We can then conclude that the enhancement in ω_{cutoff} with n, caused by the field inhomogeneity, would decrease for $n \gg 1$. Figure 5 shows that there is a dramatic increase in ω_{cutoff} for $n = 1$ and $n = 2$, and a small increase for $n = 3$, over those of the conventional laser-field case. However, in agreement with our previous statements, the influence of the field inhomogeneity drops considerably for $n > 3$.

For practical reasons, we examine the n-scaling of the HHG cutoff position q_{cut} with respect to the bound-states $n = 1$–8 of our 1D model atom. Using the three-step model for the Rydberg-like series, with the n^{-2} bound-state scaling, we observe that ω_{cutoff} scales as n^{-2}, therefore the HHG cutoff position is $q_{\text{cut}} = \omega_{\text{cutoff}}/\omega_0 \sim n$ [47]. Then we can deduce that the scaled HHG cutoff position can be written as

$$\frac{q_{\text{cut}}}{n} = \text{const}, \tag{15}$$

which should exactly be satisfied for $E_n \sim n^{-2}$ [47]. Figure 6 shows the variation of the scaled cutoff (q_{cut}/n ratio) for spatially homogeneous ($\beta = 0$) and inhomogeneous ($\beta = 0.016$ a.u.) fields. As shown, the scaled HHG cutoff for $\beta = 0$ increases with n and converges to a constant value in accordance with Eq. (15). In our simulations we find that, in agreement with the three-step model, $q_{\text{cut}}/n \to 32$ for $n \gg 1$. For $\beta = 0.016$ a.u., however, the condition provided in Eq. (15) is not fulfilled, due to the nonponderomotive character of the

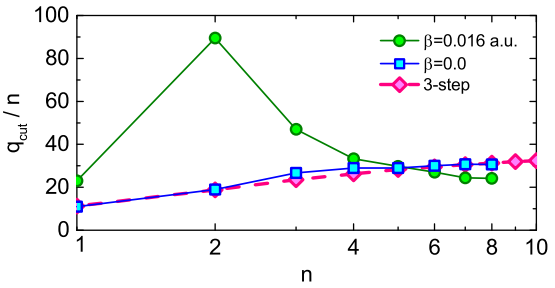

FIG. 6. Variation of the scaled cutoff position $q_{\rm cut}/n$ with n. The dashed line with diamonds represents the three-step model's predictions; the solid line with squares, our TDSE results for the spatial homogeneous field, $\beta = 0$, respectively. Open circles represent the $q_{\rm cut}/n$ ratio for plasmon-enhanced HHG with $\beta = 0.016$ a.u. Symbols are connected by lines as a guide for the eye.

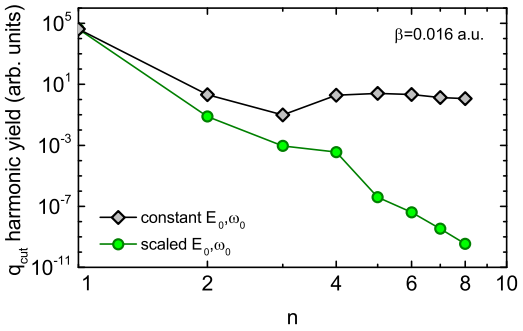

FIG. 7. n scaling of the $q_{\rm cut}$ harmonic efficiency for $\beta = 0.016$ a.u. The values of E_0 and ω_0 are those presented in Figs. 2 and 5 for constant and scaled field parameters, respectively.

electron acceleration [64]. On the other hand, although for $\beta = 0.016$ a.u. we stated that the influence of the nanostructure element diminishes for higher values of n, we can clearly see here that beyond $n = 5$ the cutoff position is close, but it begins to deviate slightly from those predicted by the three-step model and/or our TDSE simulations for $\beta = 0$. This behavior arises because the initial width of the wave packet approaches the metal's surfaces for higher values of n, increasing the chances of surface absorption of energetic electrons with a high linear momentum [21,23,26].

C. n-scaling of the plasmonic-HHG yield

So far we have demonstrated HHG from a Rydberg atom in spatially inhomogeneous laser fields for constant or n-scaled laser-field parameters (E_0 and ω_0). However, one can ask the question, Which of these two procedures is more beneficial in terms of conversion efficiency? This is investigated in terms of the interplay among the maximum photon energies, their yields, and the probability of reaching the nanostructure material damage threshold.

It has been noted that, for conventional (spatially homogeneous) strong-field interactions, the efficiency of harmonics in HHG is inversely proportional to the degree of the electron wave-packet transverse spread at the time of recombination with the parent ion [4,65,66]:

$$\sigma_x \propto \frac{E_0^{1/2}}{I_p^{1/4}\omega_0}. \tag{16}$$

As n increases, the wave-packet spread scales as

$$\sigma_x = n^{3/2}\widetilde{\sigma}_x \tag{17}$$

for fixed E_0 and ω_0 and as

$$\sigma_x = n^{1/2}\widetilde{\sigma}_x \tag{18}$$

for n-scaled E_0 and ω_0. We can see that the electron wave-packet spread increases, and thus the efficiency of harmonics for conventional laser fields decreases, with n for both constant and scaled field parameters. However, the decay is relatively faster for the scaled ones. In Fig. 7, the same asseveration applies for plasmon-enhanced laser fields, although the variation in harmonic efficiency of $q_{\rm cut}$ is not very regular. For constant laser-field parameters, the harmonic yield drops, then saturates after $n = 3$, in accordance with what is shown in Fig. 3. On the other hand, for scaled parameters, the decrease in yield is even more dramatic as n grows.

There is clearly no benefit in using very-high-n states, for plasmonic HHG near the metallic nanostructure, in terms of the maximum photon energies and their yields (see also Figs. 2 and 5). For the $n = 2$–8 series with constant E_0 and ω_0, the harmonic yields are relatively high compared with those for scaled E_0 and ω_0 (see Fig. 7). As previously stated, however, the plasmon-enhanced fields employed for these n states are self-detrimental. We note that plasmonic HHG from $n = 2$ with scaled field parameters appears to be the best option among the whole studied series.

IV. PLASMONIC HHG FROM A REAL H ATOM IN THREE DIMENSIONS

In this section, we address whether some of the assessments of plasmonic HHG in a 1D model atom apply in more realistic situations. For this, we perform simulations for the plasmonic HHG from a real H atom in three dimensions. To this end we restrict our calculations to the ground ($1s$) and first excited ($2s$) states, since, as shown in the Sec. III, there might be no benefit in going beyond $n = 2$ in terms of the plasmonic-HHG efficiency and maximum photon energy.

Figures 8(a)–8(c) show the results of our simulations. We first use $I = 20$ TW/cm^2 and $\lambda = 800$ nm for an H atom in a $1s$ state [Fig. 8(a)] and scale these parameters with n^{-8} and n^3 for the $2s$-state case, respectively. Thus, the field parameters become $I = 20 \times 2^{-8} = 0.078$ TW/cm^2 and $\lambda = 800 \times 2^3 = 6400$ nm, respectively [Fig. 8(b)]. For these two cases we use $\beta = 0.016$ a.u. and the laser intensities are enhanced up to 300 and 1.2 TW/cm^2 near the metal surfaces, respectively. For the selected laser-field parameters, the maximum photon energies predicted by the three-step model, for the $1s$ and $2s$ states, are 17 and 4.35 eV, respectively. However, as shown in Fig. 8(a), when the H atom in the ground state is exposed to a plasmon-enhanced field with $\beta = 0.016$ a.u., the plateau is extended up to ~ 23 eV. This value is slightly smaller than that for the 1D model atom in the ground state (see Fig. 5). This can be attributed to the limitations of the 1D model's ability to describe the transversal spreading of the electron wave packet. Note that the binding energy (and also the I_p) of the 1D model atom in the ground state is the same as that of the real H atom

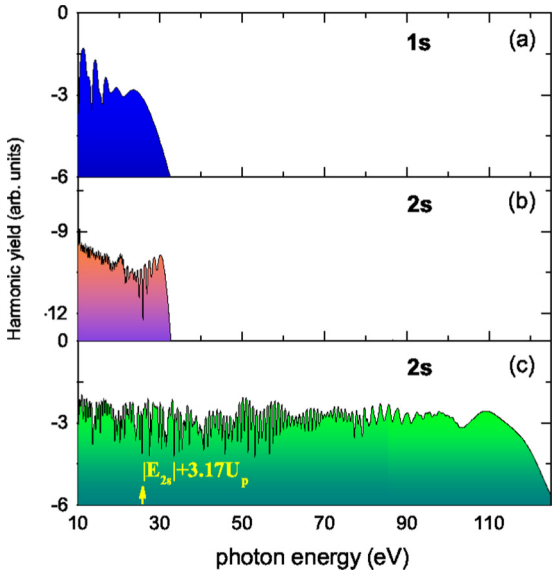

FIG. 8. Plasmonic-HHG harmonic yield vs harmonic order (ω/ω_0) for different n states obtained from a real H atom in three dimensions. (a) Ground-state ($1s$) H exposed to a plasmon-enhanced field with a field inhomogeneity parameter $\beta = 0.016$ a.u., intensity $I = 20$ TW/cm^2, and $\lambda = 800$ nm. (b) Plasmonic HHG from a H atom in the $2s$ state, again with $\beta = 0.016$ a.u. For the $2s$ state, the plasmonic field parameters are scaled to those in (a); i.e., I is multiplied by 2^{-8} ($I = 0.078$ TW/cm^2), and λ by 2^3 ($\lambda = 6400$ nm). (c) Plasmonic HHG from a $2s$ state with $I' = 2$ TW/cm^2 and $\lambda = 6400$ nm. The three-step model with $\beta = 0$ predicts an HHG cutoff at 17 eV (a), 4.3 eV (b), and 28 eV (c) [3,4].

in three dimensions. For the $2s$ state, shown in Fig. 8(b), we observe a plasmonic HHG extending from the theoretically predicted value of 4.35 eV (for $\beta = 0$) to 30 eV. However, compared with the $1s$-state case, the efficiency of the plateau drops almost seven orders of magnitude. This decrease is a consequence of the increase in the transversal spreading of the electron wave packet in the continuum upon going from the $1s$ to the $2s$ state [see Eqs. (16)–(18)].

Finally, we demonstrate plasmonic HHG from a $2s$ state using a laser field whose intensity is stronger than $I = 0.078$ TW/cm^2 but still well below the damage threshold. Here we use $I' = 2$ TW/cm^2 for an H atom in a $2s$ state with a laser wavelength $\lambda = 6400$ nm (6.4 μm; the corresponding $\omega_0 = 0.194$ eV) [Fig. 8(c)]. The three-step model predicts a value of $\omega_{\text{cutoff}} = 26$ eV for a spatially homogeneous laser field [3,4]. As shown in Fig. 8(c), a 25-fold increase in intensity results in a roughly 4-fold extension of the plateau region for this $2s$ state. Moreover, the efficiency of the plasmonic-HHG approaches that for the $1s$ state [see Fig. 8(a)]. This example clearly shows the benefit of employing Rydberg atoms in plasmonic HHG. However, in general, the interplay between the propagation time and the spatial extension of the electron wave packet, together with the possibility of absorption of the continuum electron at metal surfaces during its excursion, should to be considered. Furthermore, techniques for preventing damage to the nanostructure element are among the most crucial phenomena to exploit the maximum efficiency of plasmonic HHG by Rydberg atoms.

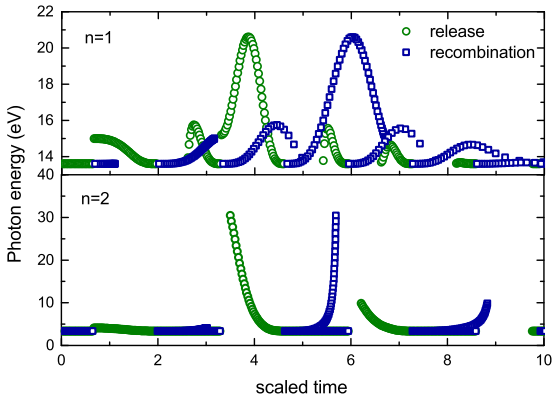

FIG. 9. Semiclassical simulations for an electron in a plasmonic field. The graph shows the electron kinetic energy at recombination as a function of the release t_i and recombination t_r times in *scaled* units (fs/n^3). It is assumed that the electron is released from $n = 1$ (top) and $n = 2$ (bottom) states. For $n = 1$, $\beta = 0.016$ a.u., intensity $I = 20$ TW/cm^2, and $\lambda = 800$ nm. For $n = 2$, again $\beta = 0.016$ a.u. and the plasmonic field parameters are correspondingly scaled to those in the top panel, i.e., I by 2^{-8} and λ by 2^3. The three-step model with $\beta = 0$ predicts cutoffs at 17 and 4.3 eV for $n = 1$ and 2, respectively.

V. SEMICLASSICAL PLASMONIC HHG

In this section, we perform semiclassical simulations extended to atoms in a plasmon-enhanced field [21–23,67]. In order to simulate Rydberg atoms we consider two cases; the electron is released either from an $n = 1$ state or from an $n = 2$ state. For $n = 2$, the laser parameters and the energy levels are scaled to those of $n = 1$. The motion of the semiclassical electron under the influence of a plasmonic laser field is described by

$$\ddot{x}(t) = (1 + 2\beta x)E(t), \tag{19}$$

where $E(t)$ is defined in Sec. II. The semiclassical equation is numerically solved by the velocity Verlet algorithm. The electron is released at time t_i and position $x_n(t_i) = 3n^2/2$ with zero kinetic energy and travels under the influence of the laser electric field. Here, x_n is the expectation value of the semiclassical electron bound to the nth state of a H atom. On the other hand, due to the possibility of electron absorptions at metal surfaces, we make sure that the trajectories that reach the metallic surfaces are neglected [21]. For those electrons which return and recombine with the parent ion at time t_r, the total energy is then $|E_n| + E_k(t_r)$, where $E_n = -0.5/n^2$ is the potential energy of the nth level of the H atom and $E_k(t_r)$ is the kinetic energy of the recombined electron.

Figure 9 shows the electron kinetic energy at the recombination, i.e., the harmonic photon energy, in terms of the harmonic order, as a function of the release (ionization) t_i and recombination t_r *scaled* times (i.e., in units of fs/n^3), for both $n = 1$ and $n = 2$. For $n = 1$, the maximum energy is 21 eV, which is in very good agreement with that predicted by the 3D TDSE [see Fig. 8(a)] and marginally lower than the energy obtained with the 1D model atom. For $n = 2$, on the other hand, semiclassical simulations predict a maximum photon energy of 31.3 eV. This value agrees well with the 3D TDSE

prediction ($\sim$ 30 eV) and, again, is slightly lower than in the 1D TDSE case ($\sim$ 35 eV). As already mentioned, we inferred that the disagreement between the 1D and the 3D quantum models is due to the lateral spreading of the electron wave packet, which is apparently missing or underestimated in the 1D case.

Although they are not shown here, we also find that the maximum photon energies decrease dramatically for $n > 2$ states. This is consistent with the conclusions we have reached for the 1D TDSE case (see Fig. 5).

VI. CONCLUDING REMARKS

In conclusion, we have presented a complete theoretical investigation of the behavior of Rydberg atoms in plasmon-enhanced laser fields producing so-called plasmonic HHG. Since scaling is crucial in this context, as we increase the principal quantum number of the initial Rydberg state n, we systematically n-scale the laser input parameters, such as the incident field strength and frequency. We have simulated plasmonic HHG based on the numerical solution of the TDSE for a 1D model atom and a real H atom in three dimensions.

We have first simulated plasmonic HHG from Rydberg atoms with a fixed laser-field intensity and frequency. We have found that in the case of spatially homogeneous (conventional) laser fields the dynamics of ionization is governed by the mechanism of barrier suppression (BSI) for $n > 1$. However, when we place the Rydberg atoms in a spatially inhomogeneous plasmon-enhanced field, we observe that ionization rates decrease by several orders of magnitude. This is caused by the electron confinement in a nano-volume; recombination of the laser-ionized electron is then possible, and therefore HHG plausible. This contrasts with the case of Rydberg atoms in conventional fields, where recombination is strongly suppressed.

We have then n-scaled both the field intensity and the frequency of the driving laser field as n increases. We have observed a maximum cutoff enhancement by the $n = 2$ state. Beyond that point, the influence of the plasmon-enhanced field is no longer substantial.

Finally, in order to complement our assessments, we have also employed the TDSE in three dimensions for a H atom in a spatially inhomogeneous plasmon-enhanced field and simulated plasmonic HHG from the ground ($1s$) and the first excited ($2s$) states. We have verified that the length of the plateau is of the same order for both $1s$ and $2s$ states, where the field parameters are n-scaled over those of the $1s$ state. Semiclassical simulations have revealed that the maximum photon energies for both the $n = 1$ and the $n = 2$ states agree very well with the 3D simulations and are marginally lower than those of the 1D approach, thus suggesting that lateral spreading of the electron wave packet appears to be critical in this process.

ACKNOWLEDGMENTS

Y.T. and Z.A. acknowledge support from BAPKO of Marmara University. The authors are grateful to Dr. E. A. Bleda for helpful discussions and a critical reading of the manuscript. M.L. and A.C. acknowledge the support of Spanish MINECO (Nacional Plan Grant Foqus FIS2013-46768-P), Severo Ochoa (Grant No. SEV-2015-0522), Fundació Cellex, Catalan AGAUR (SGR 2014 874), and ERC AdG OSYRIS.

[1] P. B. Corkum and F. Krausz, Nat. Phys. **3**, 381 (2007).
[2] T. Brabec and F. Krausz, Rev. Mod. Phys. **72**, 545 (2000).
[3] P. B. Corkum, Phys. Rev. Lett. **71**, 1994 (1993).
[4] M. Lewenstein, Ph. Balcou, M. Yu. Ivanov, A. L'Huillier, and P. B. Corkum, Phys. Rev. A **49**, 2117 (1994).
[5] M. Lewenstein and A. L'Huillier, in *Strong Field Laser Physics*, edited by T. Brabec (Springer-Verlag, New York, 2009), pp. 147–183.
[6] M. B. Gaarde, J. L. Tate, and K. J. Schafer, J. Phys. B **41**, 132001 (2008).
[7] A. Sanpera, P. Jönsson, J. B. Watson, and K. Burnett, Phys. Rev. A **51**, 3148 (1995).
[8] J. Tate, T. Auguste, H. G. Muller, P. Salières, P. Agostini, and L. F. DiMauro, Phys. Rev. Lett. **98**, 013901 (2007).
[9] C. Gohle, T. Udem, M. Herrmann, J. Rauschenberger, R. Holzwarth, H. A. Schuessler, F. Krausz, and T. W. Hänsch, Nature **436**, 234 (2005).
[10] D. Strickland and G. Mourou, Opt. Commun. **55**, 447 (1985).
[11] J. A. Schuller, E. S. Barnard, W. Cai, Y. C. Jun, J. S. White, and M. L. Brongersma, Nat. Mater. **9**, 193 (2010).
[12] S. Kim, J. Jin, Y.-J. Kim, I.-Y. Park, Y. Kim, and S.-W. Kim, Nature **453**, 757 (2008).
[13] I.-Y. Park, S. Kim, J. Choi, D.-H. Lee, Y.-J. Kim, M. F. Kling, M. I. Stockman, and S.-W. Kim, Nat. Photon. **5**, 677 (2011).
[14] M. Sivis, M. Duwe, B. Abel, and C. Ropers, Nat. Phys. **9**, 304 (2013).
[15] N. Pfullmann, C. Waltermann, M. Noack, S. Rausch, T. Nagy, C. Reinhardt, M. Kovačev, V. Knittel, R. Bratschitsch, D. Akemeier, A. Hütten, A. Leitenstorfer, and U. Morgner, New J. Phys. **15**, 093027 (2013).
[16] I.-Y. Park, J. Choi, D.-H. Lee, S. Han, S. Kim, and S.-W. Kim, Ann. Phys. (Berlin) **525**, 87 (2013).
[17] E. Hutter and J. H. Fendler, Adv. Mater. **16**, 1685 (2004).
[18] L. Keldysh, Sov. Phys. JETP **20**, 1307 (1965).
[19] C. Blaga, F. Catoire, P. Colosimo, G. Paulus, H. Muller, P. Agostini, and L. DiMauro, Nat. Phys. **5**, 335 (2009).
[20] B. Fetić, K. Kalajdžić, and D. B. Milošević, Ann. Phys. (Berlin) **525**, 107 (2013).
[21] A. Husakou, S.-J. Im, and J. Herrmann, Phys. Rev. A **83**, 043839 (2011).
[22] M. F. Ciappina, J. Biegert, R. Quidant, and M. Lewenstein, Phys. Rev. A **85**, 033828 (2012).
[23] I. Yavuz, E. A. Bleda, Z. Altun, and T. Topcu, Phys. Rev. A **85**, 013416 (2012).
[24] J. A. Pérez-Hernández, M. F. Ciappina, M. Lewenstein, L. Roso, and A. Zaïr, Phys. Rev. Lett. **110**, 053001 (2013).
[25] M. F. Ciappina, T. Shaaran, and M. Lewenstein, Ann. Phys. (Berlin) **525**, 97 (2013).
[26] I. Yavuz, Phys. Rev. A **87**, 053815 (2013).

[27] C. Zhang, C. Liu, and Z. Xu, Phys. Rev. A **88**, 035805 (2013).
[28] L. He, Z. Wang, Y. Li, Q. Zhang, P. Lan, and P. Lu, Phys. Rev. A **88**, 053404 (2013).
[29] J. Luo, Y. Li, Z. Wang, L. He, Q. Zhang, P. Lan, and P. Lu, Phys. Rev. A **89**, 023405 (2014).
[30] H. Ebadi, Phys. Rev. A **89**, 053413 (2014).
[31] M. Lupetti, M. F. Kling, and A. Scrinzi, Phys. Rev. Lett. **110**, 223903 (2013).
[32] S. L. Stebbings, F. Süßmann, Y. Y. Yang, A. Scrinzi, M. Durach, A. Rusina, M. I. Stockman, and M. F. Kling, New J. Phys. **13**, 073010 (2011).
[33] M. Sivis and C. Ropers, Phys. Rev. Lett. **111**, 085001 (2013).
[34] T. Shaaran, M. F. Ciappina, R. Guichard, J. A. Pérez-Hernández, L. Roso, M. Arnold, T. Siegel, A. Zaïr, and M. Lewenstein, Phys. Rev. A **87**, 041402 (2013).
[35] A. Husakou and J. Herrmann, Phys. Rev. A **90**, 023831 (2014).
[36] S. Sakabe, C. Lienau, and R. Grunwald, *Progress in Nonlinear Nano-Optics* (Springer International, Cham, Switzerland, 2015).
[37] M. Sivis, M. Duwe, B. Abel, and C. Ropers, Nature **485**, E1 (2012).
[38] T. Shaaran, M. F. Ciappina, and M. Lewenstein, J. Mod. Opt. **59**, 1634 (2012).
[39] M. B. Raschke, Ann. Phys. (Berlin) **525**, A40 (2013).
[40] J. B. Watson, A. Sanpera, X. Chen, and K. Burnett, Phys. Rev. A **53**, R1962 (1996).
[41] A. Sanpera, J. B. Watson, M. Lewenstein, and K. Burnett, Phys. Rev. A **54**, 4320 (1996).
[42] P. Moreno, L. Plaja, and L. Roso, Phys. Rev. A **55**, R1593(R) (1997).
[43] D. Milošević and F. Ehlotzky, in *Advances in Atomic, Molecular and Optical Physics*, edited by B. Bederson and H. Walther (Elsevier Academic Press, Amsterdam, 2003), pp. 373–532.
[44] D. Milošević, J. Opt. Soc. Am. B **23**, 308 (2006).
[45] X. Yuan, P. Wei, C. Liu, Z. Zeng, Y. Zheng, J. Jiang, X. Ge, and R. Li, Appl. Phys. Lett. **107**, 041110 (2015).
[46] T. F. Gallagher, *Rydberg Atoms* (Cambridge University Press, Cambridge, UK, 1994).
[47] E. A. Bleda, I. Yavuz, Z. Altun, and T. Topcu, Phys. Rev. A **88**, 043417 (2013).
[48] N. Vitanov, K. Suominen, and B. Shore, J. Phys. B **32**, 4535 (1999).
[49] F. Vewinger, M. Heinz, R. G. Fernandez, N. V. Vitanov, and K. Bergmann, Phys. Rev. Lett. **91**, 213001 (2003).
[50] N. Vitanov, T. Halfmann, B. Shore, and K. Bergmann, Annu. Rev. Phys. Chem. **52**, 763 (2001).
[51] K. Bergmann, N. V. Vitanov, and B. W. Shore, J. Chem. Phys. **142**, 170901 (2015).
[52] M. F. Ciappina, S. S. Aćimović, T. Shaaran, J. Biegert, R. Quidant, and M. Lewenstein, Opt. Express **20**, 26261 (2012).
[53] I. Yavuz, Y. Tikman, and Z. Altun, Phys. Rev. A **92**, 023413 (2015).
[54] M. Protopapas, C. H. Keitel, and P. L. Knight, Rep. Prog. Phys. **60**, 389 (1997).
[55] Q. Su and J. H. Eberly, Phys. Rev. A **44**, 5997 (1991).
[56] J. L. Krause, K. J. Schafer, and K. C. Kulander, Phys. Rev. A **45**, 4998 (1992).
[57] K. Burnett, V. C. Reed, J. Cooper, and P. L. Knight, Phys. Rev. A **45**, 3347 (1992).
[58] D. Bauer, Phys. Rev. A **55**, 2180 (1997).
[59] R. Shakeshaft, R. M. Potvliege, M. Dörr, and W. E. Cooke, Phys. Rev. A **42**, 1656 (1990).
[60] W. L. Barnes, A. Dereux, and T. W. Ebbesen, Nature **424**, 824 (2003).
[61] S. Eustis and M. A. El-Sayed, Chem. Soc. Rev. **35**, 209 (2006).
[62] K. A. Willets and R. P. Van Duyne, Annu. Rev. Phys. Chem. **58**, 267 (2007).
[63] M. V. Ammosov, N. B. Delone, and V. P. Kraĭnov, Zh. Eksp. Teor. Fiz. **91**, 2008 (1986) [Sov. Phys. JETP **64**, 1191 (1986)].
[64] G. Herink, D. Solli, M. Gulde, and C. Ropers, Nature **483**, 190 (2012).
[65] N. Delone and V. P. Krainov, J. Opt. Soc. Am. B **8**, 1207 (1991).
[66] M. Y. Ivanov, T. Brabec, and N. Burnett, Phys. Rev. A **54**, 742 (1996).
[67] M. F. Ciappina, J. A. Pérez-Hernández, and M. Lewenstein, Comput. Phys. Commun. **185**, 398 (2014).